Advances in Structural Engineering

Hybrid Simulation of Structure to Tsunami Loading

Journal:	*Advances in Structural Engineering*
Manuscript ID	ASE-18-0520.R4
Manuscript Type:	Original Research
Date Submitted by the Author:	02-May-2019
Complete List of Authors:	Forouzan, Bahareh; Clarkson University, Civil Engineering Baragamage, Dilshan; Clarkson University, Civil Engineering Shaloudegi, Koushyar; Clarkson University, Civil Engineering Nakata, Narutoshi; University of Tokushima, Civil Engineering Wu, Weiming; Clarkson University, Civil Engineering
Keywords:	Hybrid simulation, structural assessment, fluid-structure interaction, coastal hazard, force-based approach, Numerical integration algorithm
Abstract:	A new hybrid simulation technique has been developed to assess the behavior of a structure under hydrodynamic loading. It integrates the computational fluid dynamics and structural hybrid simulation and couples the fluid loading and structure response at each simulation step. The conventional displacement-based and recently developed force-based hybrid simulation approaches are adopted in the structural analysis. The concept, procedure, and required components of the proposed hybrid simulation are introduced in this paper. The proposed hybrid simulation has been numerically and physically tested in case of a coastal building impacted by a tsunami wave. It is demonstrated that the force error in the displacement-based approach is significantly larger than that in the force-based approach. The force-based approach allows for a more realistic and reliable structural assessment under tsunami loading.

	Fluid Simulation		Structural Simulation
Governing Equations	Flow Equations		Equation of Motion
Simulation Tools	CFD		FEM/ Experimental Testing
Data Exchanges in the Integrated Simulation	Fluid Pressure	Fluid Force →	Input Force
	Update Boundary Condition	← Structural Deformation	Output Response

Figure 1. Description of the fluid and structural simulations.

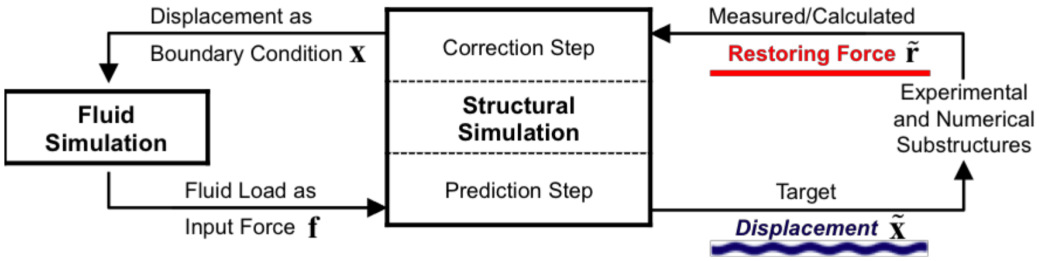

Figure 2. Data flow in the displacement-based structure-fluid hybrid simulation.

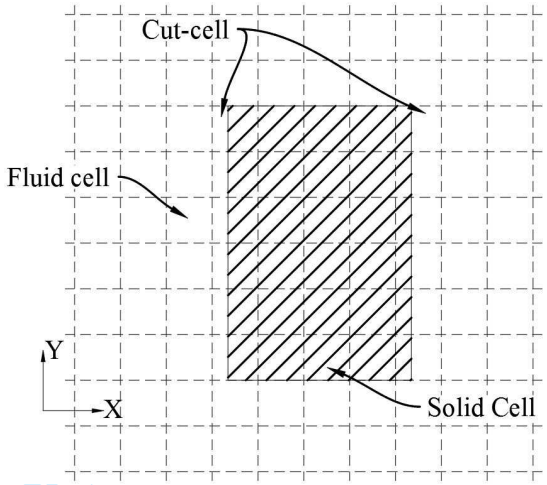

Figure 3. Cut-cells generated by a moving solid body.

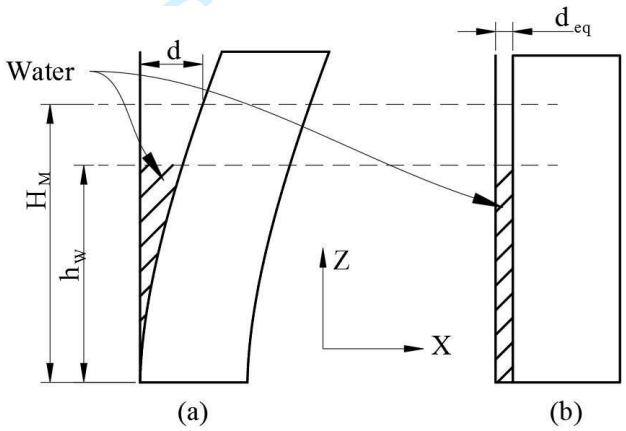

Figure 4. Deformation of the structure: (a) Actual deformation, (b) Approximated horizontal translation in the shallow water model.

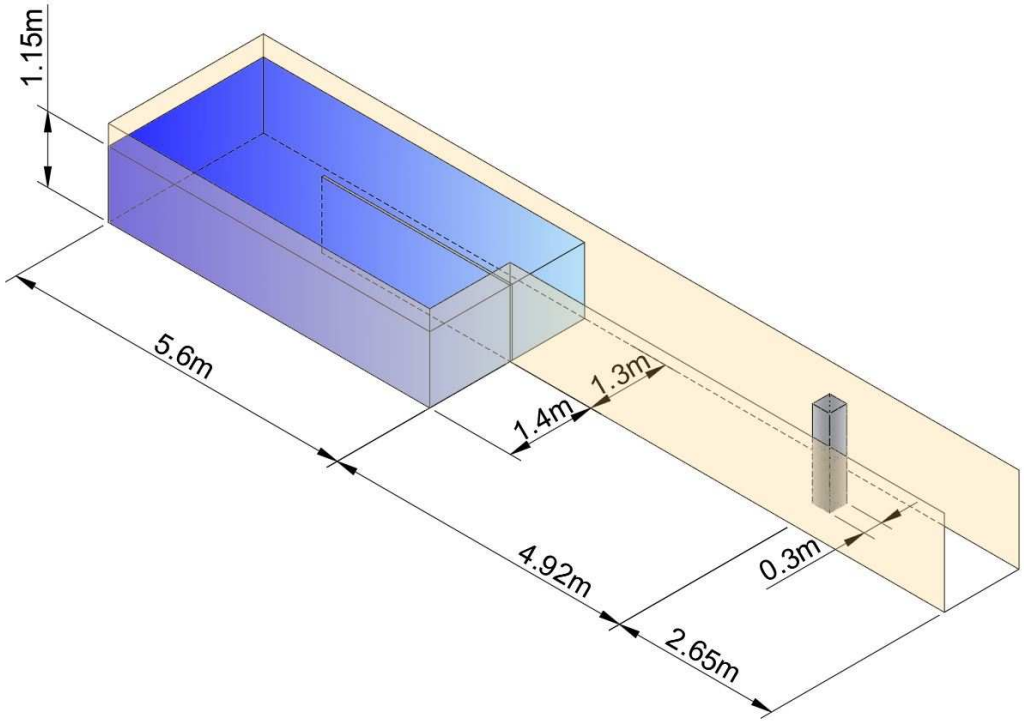

Figure 5. Experimental setup for dam-break wave impact on a rigid block.

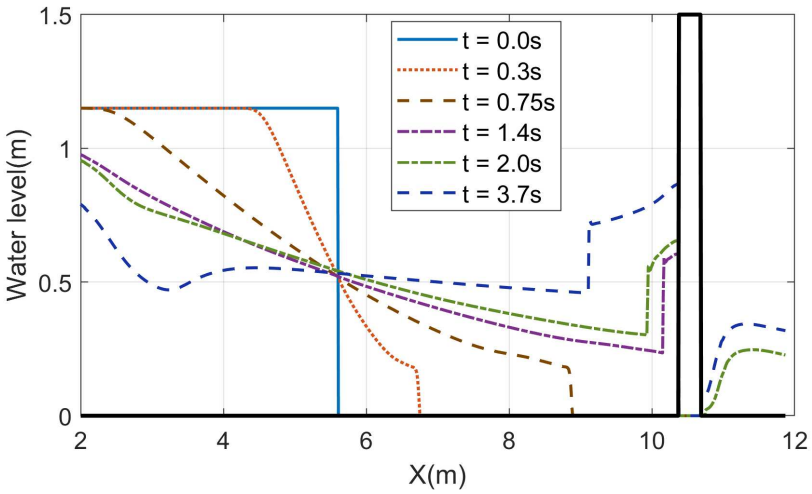

Figure 6. Calculated longitudinal profiles of dam-break wave along the centerline section of the flume.

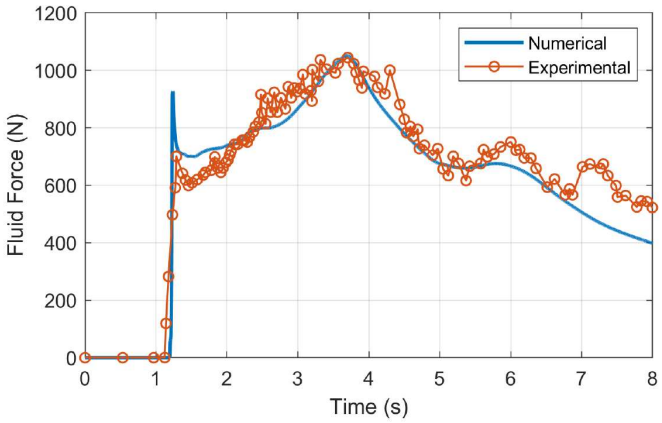

Figure 7. Comparison of calculated and measured fluid forces on the rigid block.

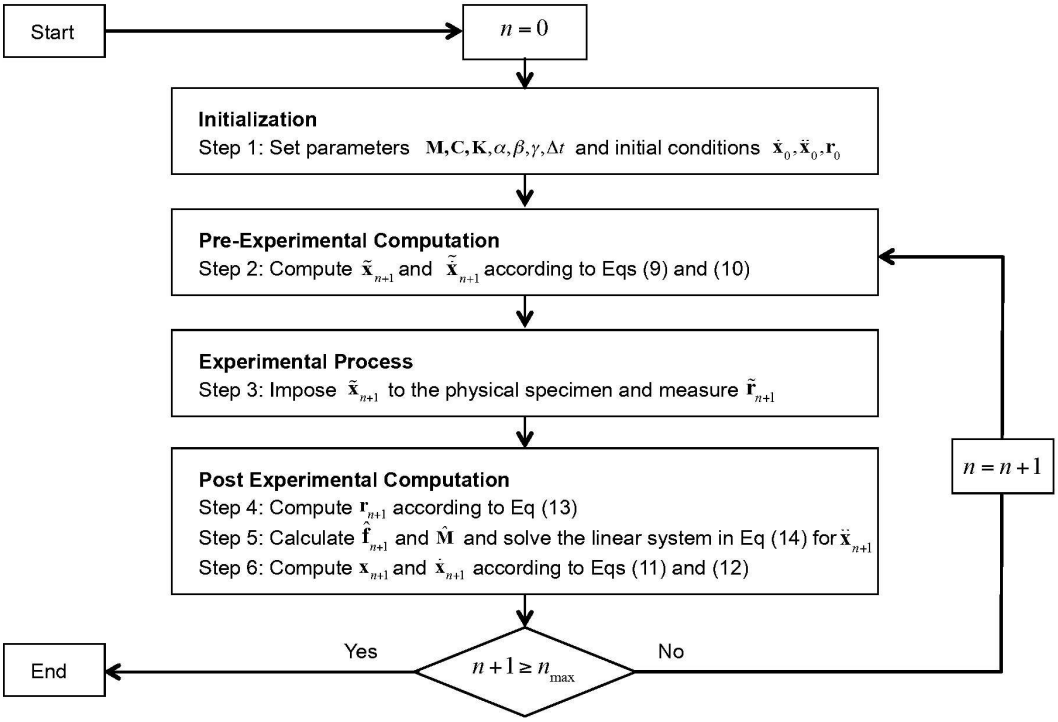

Figure 8. Implementation of the α-OS method in the displacement-based hybrid simulation.

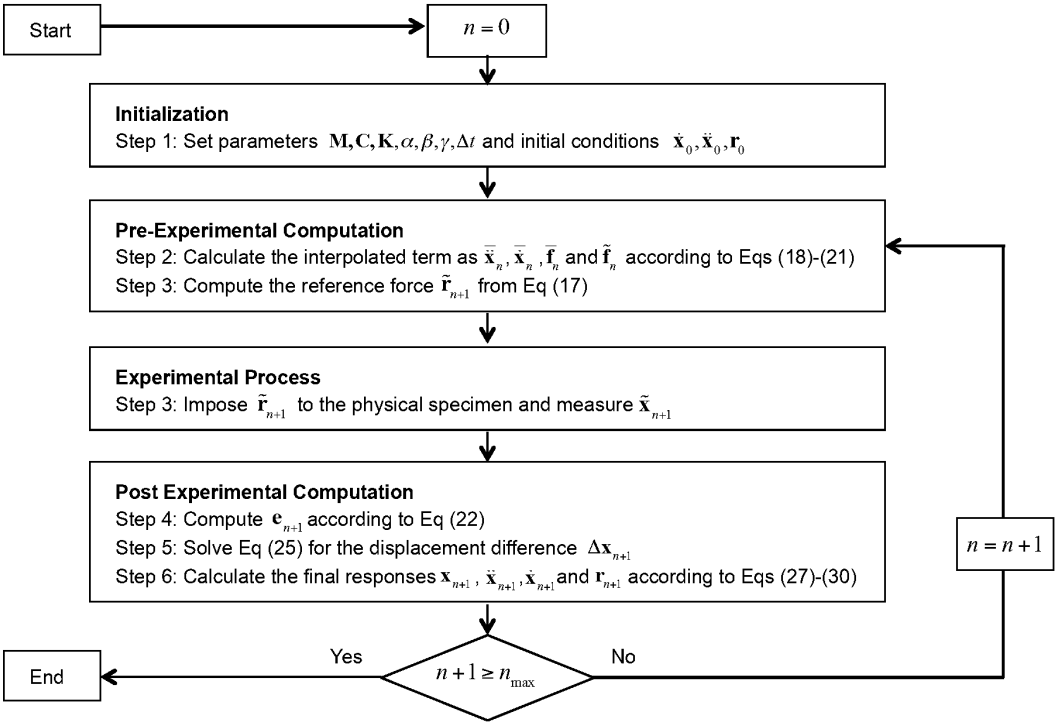

Figure 9. Implementation of the quadratic-alpha method in the force-based hybrid simulation.

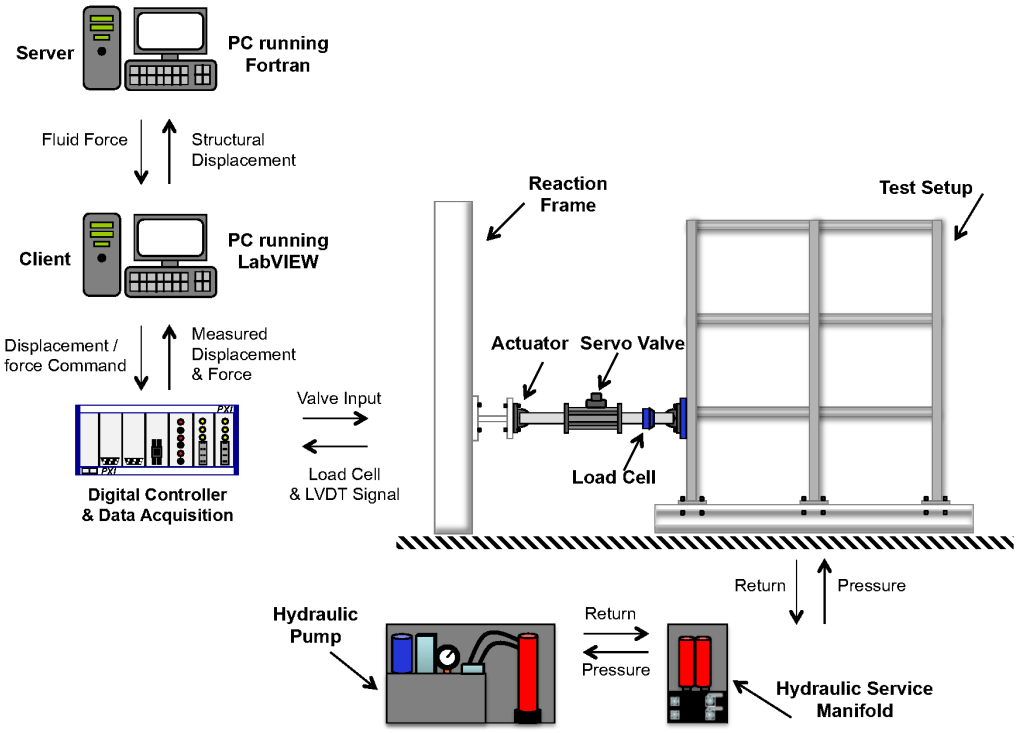

Figure 10. Schematic hardware layout of structure-fluid hybrid simulation.

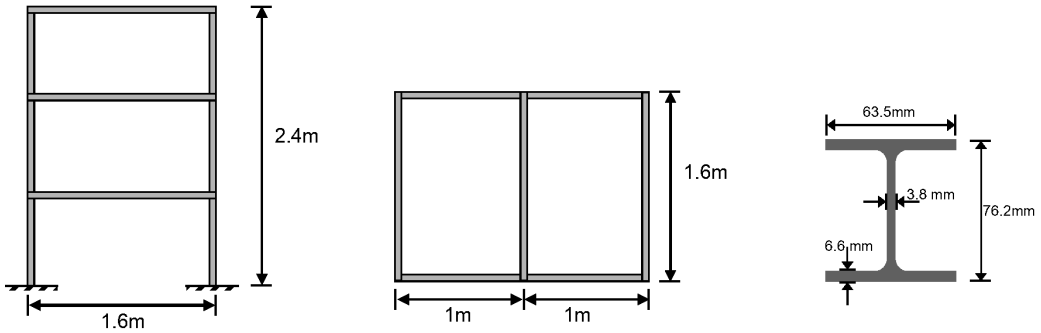

(a) Elevation (b) Floor plan (c) Beam and column section

Figure 11. Schematics of the model structure: (a) Elevation; (b) Floor plan; and (c) Beam and column section.

Figure 12. Picture of the 1:5 scaled model structure.

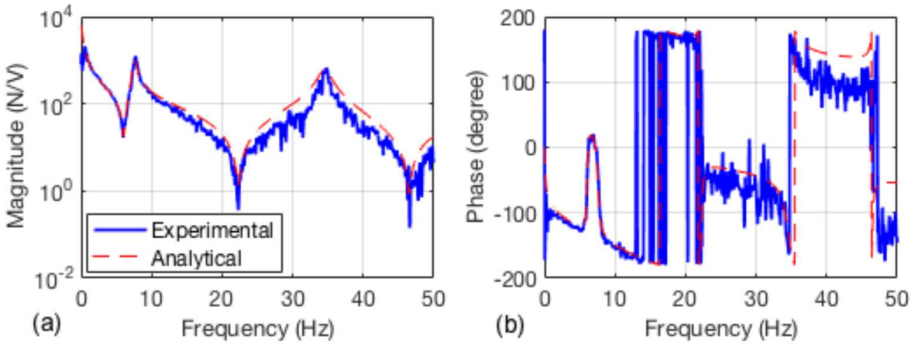

Figure 13. Dynamic characteristics of the valve command to actuator force: (a) magnitude and (b) phase.

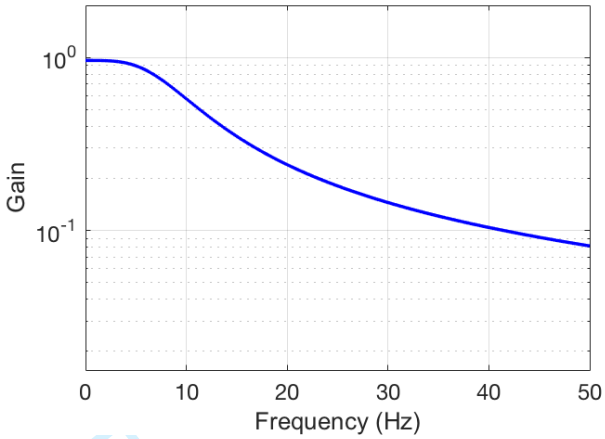

Figure 14. Closed-loop transfer function of the force controller for the test structure.

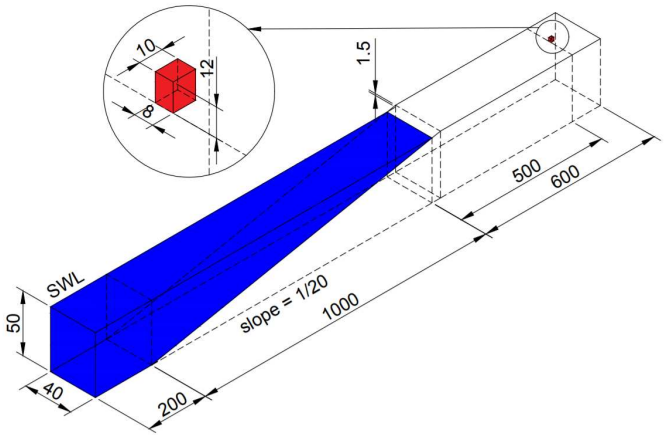

Figure 15. Fluid simulation domain (not to scale; all dimensions are in meters).

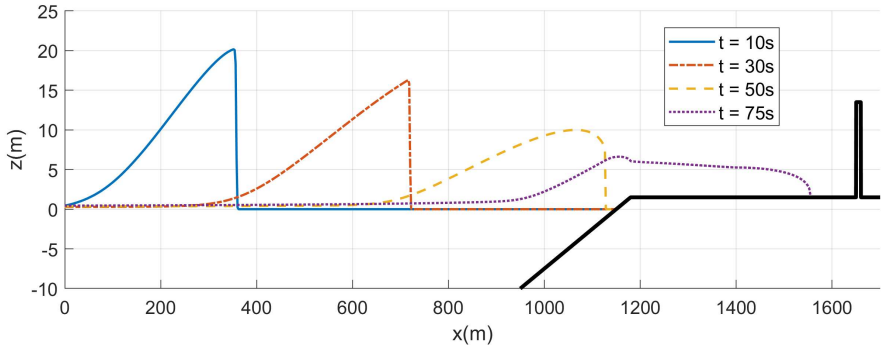

Figure 16. Wave propagation simulated with the flow model.

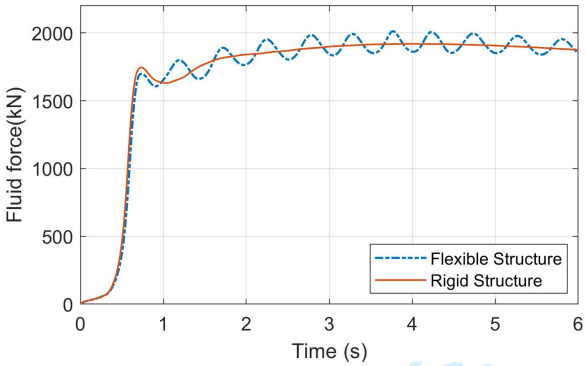

Figure 17. Comparison of fluid force on the flexible and rigid structures (time starts when the wave hits the structure).

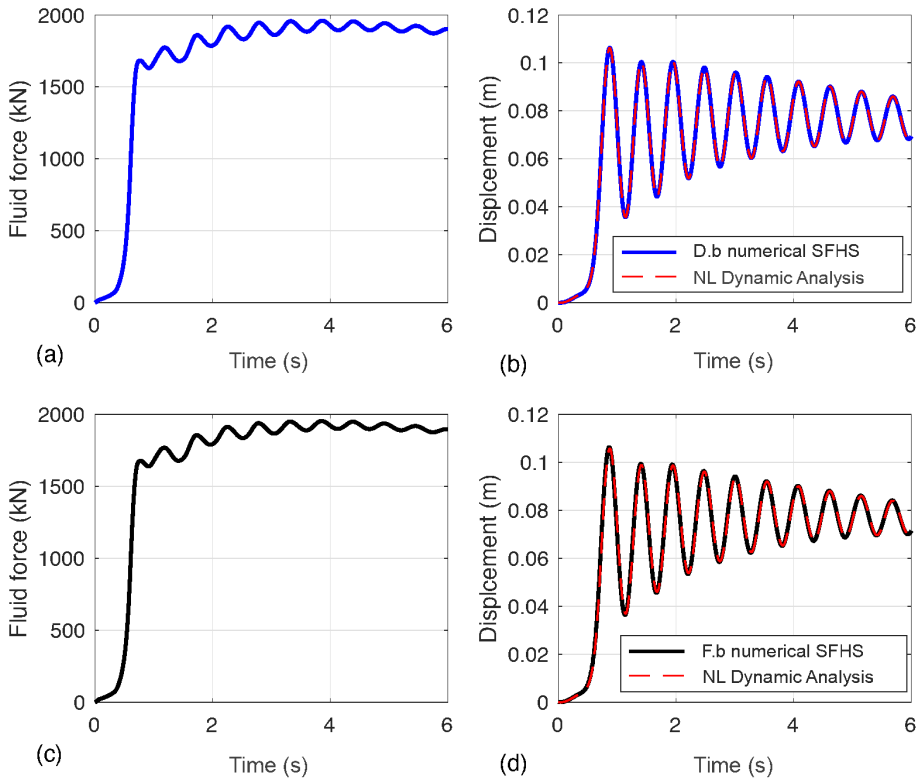

Figure 18. Results of the numerical structure-fluid hybrid simulation: (a) and (c) time histories of fluid forces in the displacement- and force-based numerical SFHS, respectively; (b) and (d) time histories of displacement in the displacement- and force-based numerical SFHS, respectively.

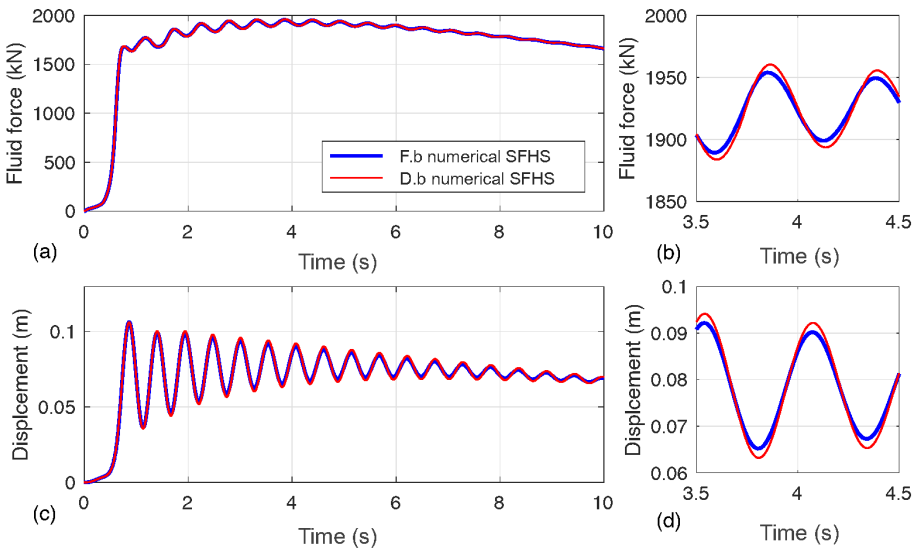

Figure 19. Comparison of the displacement- and force-based numerical structure-fluid hybrid simulations: (a) time history of input force; (b) close up view of input force; (c) time history of displacement; and (d) close up view of displacement.

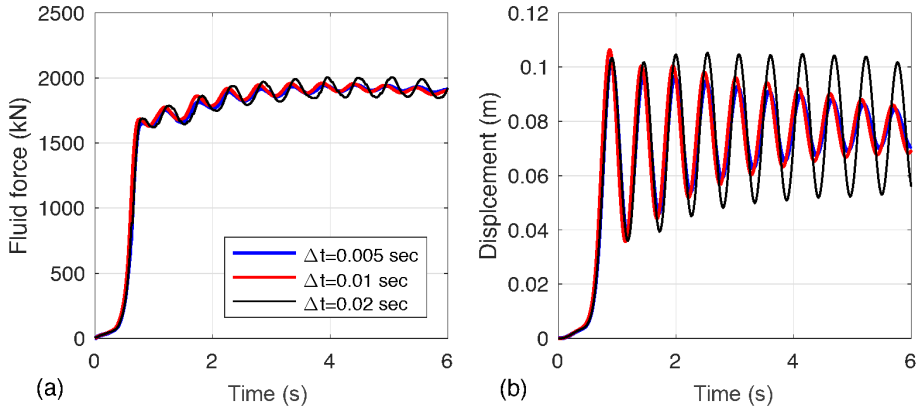

Figure 20. Influence of sampling time on the results of the displacement-based numerical structure-fluid hybrid simulation: (a) time histories of fluid force; and (b) time histories of displacement.

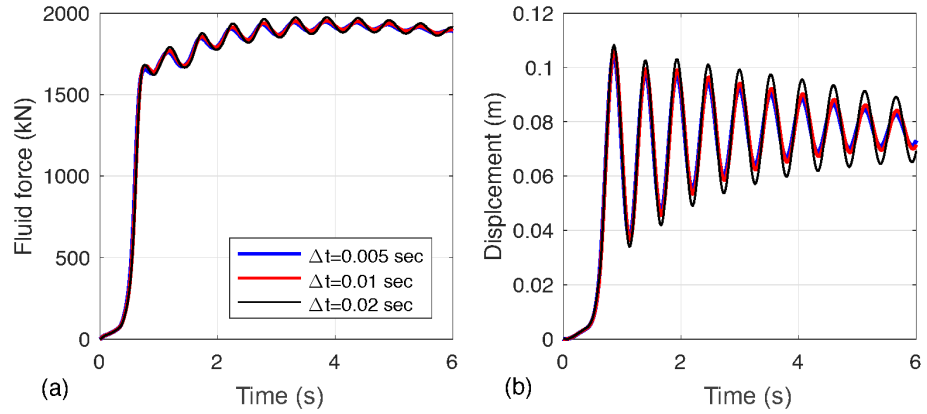

Figure 21. Influence of sampling time on the results of the force-based numerical structure-fluid hybrid simulation: (a) time histories of fluid force; and (b) time histories of displacement.

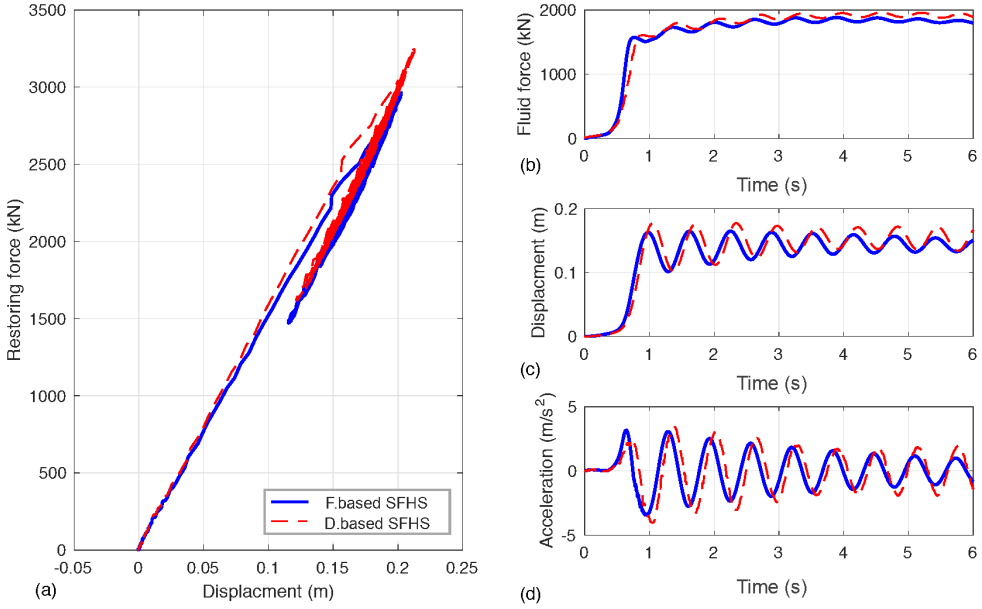

Figure 22. Comparison of experimental results in the displacement- and force-based structure-fluid hybrid simulations: (a) hysteresis; (b) fluid force time histories; (c) displacement time histories; and (d) acceleration time histories.

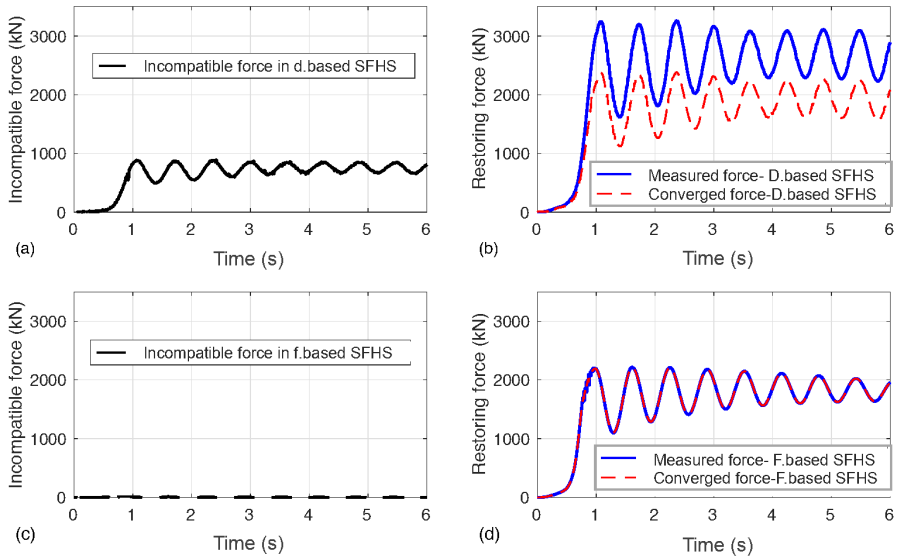

Figure 23. Various forces in the displacement- and force-based structure-fluid hybrid simulations: (a) and (c) incompatible force; (b) and (d) measured and converged forces.

Hybrid Simulation of Structure to Tsunami Loading

Bahareh Forouzan[1)], Dilshan S.P. Amarsinghe Baragamage[1)], Koushyar Shaloudegi[1)], Narutoshi Nakata[2)], and Weiming Wu[3)]

1) Graduate Student, Dept. of Civil and Environmental Engineering, Clarkson University, Potsdam, NY 13699, USA

2) Associate Professor, Dept. of Civil Engineering, Tokushima University, Japan.

3) James K. Edzwald Endowed Professor, Dept. of Civil and Environmental Engineering, Clarkson University, Potsdam, NY 13699, USA

Abstract

A new hybrid simulation technique has been developed to assess the behavior of a structure under hydrodynamic loading. It integrates the computational fluid dynamics and structural hybrid simulation and couples the fluid loading and structure response at each simulation step. The conventional displacement-based and recently developed force-based hybrid simulation approaches are adopted in the structural analysis. The concept, procedure, and required components of the proposed hybrid simulation are introduced in this paper. The proposed hybrid simulation has been numerically and physically tested in case of a coastal building impacted by a tsunami wave. It is demonstrated that the force error in the displacement-based approach is significantly larger than that in the force-based approach. The force-based approach allows for a more realistic and reliable structural assessment under tsunami loading.

Keywords

Hybrid simulation, structural assessment, fluid-structure interaction, coastal hazards

INTRODUCTION

Natural hazards, such as earthquake, tsunami, and hurricane, have caused tremendous human sufferings and extensive economic losses. In order to reduce the effects of these hazards and the vulnerabilities of structures, it is imperative to improve our knowledge and understanding of the responses of structures to such hazards. In recent years, concerns about structural integrity and risk management for coastal hazards have increased. Tsunami and flood-related loads have been addressed in several government documents, such as FEMA 55, FEMA P646 and ASCE 7-10. However, there are still

limitations in the design codes and guidelines for tsunami-induced loads. For example, some of the critical parameters, such as flow velocity, have not been thoroughly investigated.

A number of researchers have investigated coastal flood hazards by developing computational fluid dynamics (CFD) tools and conducting experiments for examination of fluid loading on structures. For example, Nistor et al. (2011) conducted experiments on tsunami loading on a structure using a high discharge flume. Winter et al. (2008) investigated the tsunami wave force on bridge components using a two-dimensional (2D) vertical flow model based on the Navier-Stokes equations. Wei et al. (2015) investigated the dynamic impact of tsunami bore on bridge piers using a smoothed particle hydrodynamics (SPH) model. Kareem (1990) performed experiments to measure and analyze the wind pressure fields and associated area-averaged loads acting on various building models in simulated atmospheric flows. Tamura et al. (1999) developed an orthogonal decomposition technique to model randomly fluctuating wind pressure fields on a structure. These advanced experimentation and modeling techniques for wind and coastal loads are promising. However, these studies usually ignored the interactions of fluid and structure.

One of the potential approaches to incorporate the interactions of fluid and structure is hybrid simulation, which is a versatile and powerful technique that evaluates the dynamic behavior of structures through numerical simulation combined with experimental testing (Hakuno et al., 1969; Takanashi and Nakashima, 1987; Shing and Mahin, 1990). One of the features of hybrid simulation is the substructuring technique, which models the structure as a combination of experimental and numerical substructures (Dermitzakis and Mahin, 1985; Thewalt and Mahin, 1987). The experimental substructures are the elements that are difficult to model numerically and are thus tested physically. The numerical substructures are the elements that are well understood or can be modeled properly using numerical analysis methods.

While hybrid simulation provides an efficient means for the dynamic analysis of structures, its application has been mainly limited to earthquake loading; few exceptions include Kato et al. (2014) that introduced a hybrid vibration technique to simulate the aerodynamic vibration of a structure, combining the numerically solved structure's equation of motion with measurement of the aerodynamic force on a model structure in a wind tunnel test. It is essential to incorporate the aforementioned fluid loading models into hybrid simulation to expand the capabilities of structural assessment for multi-hazards.

A critical feature that distinguishes coastal hazards from earthquake in hybrid simulation is the fluid-structure interactions. If the interactions are neglected, the structure can be assessed independently of the fluid motion. In this way, first, the fluid simulation is conducted to obtain the time history of fluid loading. Then, simulation is performed on the structure with the fluid loading as a prescribed input force. Such a

process is similar to the often-used earthquake simulation and would be straightforward. However, the influence of structural responses on the fluid loading is not considered (e.g., motion-induced self-excited buffeting force) (Kareem, 2008). To fully incorporate the interactions, fluid and structural simulations have to be performed in a coupled manner. Higgins et al. (2014) advanced hybrid simulation by conducting a hydrodynamic testing of wave forces on a 1:5 scale bridge deck and applying the measured time histories of wave forces to assess the performance of the connection elements of a full-scale bridge. They modeled the flexibility of bridge substructure using a pair of elastic springs connected to anchorage blocks, which could not fully account for in the fluid and structure interactions. Similar approach was developed by Istrati (2017) to assess the performance of a variety of bridge structures under different types of waves.

The present paper proposes a new hybrid simulation framework (designated as structure-fluid hybrid simulation) to assess structural responses under fluid loading. The concepts, procedures and required components to accommodate the fluid-structure interactions into the hybrid simulation are presented. The developed hybrid simulation approach is numerically and experimentally tested in an assessment of structural responses to a tsunami wave.

CONCEPT AND PROCEDURE OF STRUCTURE-FLUID HYBRID SIMULATION

Figure 1 briefly describes the governing equations, simulation tools, and data exchanges in the fluid and structure domains used by the proposed structure-fluid hybrid simulation (SFHS). The fluid and structure domains are essentially different in terms of both the employed governing equations and simulation tools. To reflect the fluid-structure interactions, the proposed hybrid simulation allows evaluation of the effects of fluid-induced force on the structural response as well as the changes of the fluid-induced force due to the structural deformation.

[insert Figure 1.]

A term “sampling time step” is introduced in the SFHS. It represents reciprocally the frequency of data exchange between the flow and structure domains. At each sampling time step, the flow governing equations are solved numerically to calculate the force induced on the structure, and then the calculated force is sent to a time stepping integration on the structure’s equation of motion as an input force. Structural simulation is performed to obtain the structure deformation, as explained in more detail in the following paragraphs. Then, the structural deformation is returned to the fluid simulation to update the boundary conditions at the next sampling time step. The whole process repeats until the end of the simulation. The sampling time step is not necessarily the same as the time steps used in the fluid model or the structural analysis.

In a conventional hybrid simulation, the displacement is calculated by solving the structure's equation of motion under an input force in a prediction/correction manner (Figure 2). Then the target displacement is imposed to the experiment through an actuator and the corresponding restoring force is measured. The output from the experiment is sent back to the time stepping integration on the structure's equation of motion, and a correction process is performed to finalize the structural responses (designated as converged responses). Herein, this method is referred to as displacement-based hybrid simulation because both formulation and control system are based on displacement. This approach has been widely applied to study the responses of structures under seismic loading, in which the dynamic loading is almost independent of the structure's deformation. It is adopted in the present fluid-structure hybrid simulation as shown in Figure 2.

[insert Figure 2.]

In the case of fluid loading, the most natural way to handle the fluid-structure boundaries is to apply the force from the fluid domain to the structural domain and then update the fluid boundary conditions using the deformation obtained in the structural simulation. However, the conventional displacement-based hybrid simulation may not be appropriate for such an integrated fluid-structure simulation, because it may have unavoidable errors between the measured restoring force from the experiment and the converged restoring force after the correction process at each step. These errors are herein called incompatible force, which becomes problematic when the measured force overshoots in a nonlinear region. The influence of the incompatible force propagates to the fluid simulation and is accumulated over a lapse of time. Another key factor in the structural simulation is to account for the direct impact of the fluid load on the structure. Accurate application of the fluid load, including the magnitude, contact surface, and loading pattern, is crucial for the integrated fluid-structure simulation. To meet this requirement a force-based hybrid simulation recently developed by Forouzan (2018) is also integrated into the structure analysis.

The force-based hybrid simulation consists of the force-based numerical integration of the structure's equation of motion and the dynamic force control in the experiment. The data flow in the force-based hybrid simulation is similar to Figure 2, except that the target force is calculated in the prediction step and imposed under a force control and the corresponding displacement is measured. In both approaches, correction procedures are performed on the measured responses to calculate the converged responses at the same sampling time step. Among these converged responses, the displacement is sent to the fluid simulation as a boundary condition.

The proposed SFHS is capable for both displacement-based and force-based hybrid simulations in the structure domain. Correspondingly, the scheme is named displacement- or force-based SFHS. The present study investigates the influence of both approaches on the simulation results.

NUMERICAL ALGORITHMS FOR STRUCTURE-FLUID HYBRID SIMULATION

To develop the SFHS, two sets of numerical algorithms are required, including: (i) CFD simulation with structural deformation updating capability, and (ii) numerical integration algorithm that solves the structure's equation of motion. These items are described in detail in the following subsections.

CFD Simulation with Structural Deformation Updating Capability

When a fast-moving stream of fluid is disturbed by an object, the change in momentum of the fluid stream imposes a force on the object. The change in flow parameters can be analyzed using CFD, which involves solving a set of governing equations by employing numerical methods and usually with the help of powerful computers.

The general motion of fluid in time and space can be modeled using the three-dimensional Navier-Stokes (NS) equations, which describe the conservation of mass and momentum as the fluid moves. The NS equations fall under the category of nonlinear partial differential equations. Because there is no general analytical solution for the NS equations, numerical techniques are required to find approximate solutions. Most of the existing numerical solution techniques require iterations until the desired level of accuracy is obtained. As the size of the flow domain increases, the required computational resource grows exponentially, which makes it virtually impossible to solve a large-domain flow problem in a quasi-real-time manner on a present-day personal computer (PC) or on an average workstation. In the present study, instead of the NS equations, the fluid motion is modeled with the 2D shallow water (SW) equations, which are derived by depth-averaging the NS equations under the assumption that the vertical inertial and viscous effects are negligible. The SW equations are given as

$$\frac{\partial h}{\partial t}+\frac{\partial (uh)}{\partial x}+\frac{\partial (vh)}{\partial y}=0 \tag{1}$$

$$\frac{\partial (uh)}{\partial t}+\frac{\partial (u^2h)}{\partial x}+\frac{\partial (uvh)}{\partial y}+gh\frac{\partial z_s}{\partial x}+\frac{n_m^2 gUu}{h^{1/3}}=0 \tag{2}$$

$$\frac{\partial (vh)}{\partial t}+\frac{\partial (uvh)}{\partial x}+\frac{\partial (v^2h)}{\partial y}+gh\frac{\partial z_s}{\partial y}+\frac{n_m^2 gUv}{h^{1/3}}=0 \tag{3}$$

where t is the time; x and y are the longitudinal and lateral coordinates, respectively; u and v are the flow velocities along x and y directions, respectively; h is the flow depth;

z_s is the water level above a reference datum; n_m is the Manning roughness coefficient; $U = \sqrt{u^2 + v^2}$; and g is the gravitational acceleration.

The SW equations are categorized as a set of nonlinear hyperbolic equations. They have one major drawback of being incapable of representing the vertical variation of the deformation over the structure. However, the SW equations are adequate for tsunami propagation and flood inundation (Titov and Synolakis, 1998, 1995; Yeh, 1994) and can be used to estimate the hydrodynamic loading on the structure.

A finite volume method is used to solve the SW equations, as introduced in detail by Wu et al. (2012). A collocated grid system consisting of rectangular cells is used to discretize the flow domain. The primitive variables (u, v, h) are stored at cell centers. The SW equations are integrated on each cell. The Harten-Lax-van Leer (HLL) (Harten et al., 1983) approximate Riemann solver is used to calculate the inter-cell numerical flux. The HLL solver is able to handle wave breaking. The temporal derivative is discretized using the explicit Euler scheme. The discretized equations are explicitly solved in time-marching steps.

In order to handle the structure movement, the fluid model uses a cut-cell method (Yang et al. 1997, 2000), in which the fluid grid remains stationary while the solid body (structure) moves on the fixed grid (Figure 3). One face of each cut-cell is conformal to the structure surface. As the structure moves, the cut-cell face is adjusted to track the moving boundary between the fluid and structure; thus, the neighboring fluid and solid cells may be changed to cut-cells, and vice-versa. The discretization of Eqs. (1)-(3) over the cut-cells is similar to the regular cells. On the cell face between the fluid and structure, the mass and momentum fluxes are determined as follows by using the non-slip boundary condition:

$$F_{mass} = h_W u_s \tag{4}$$

$$F_{momentum} = h_W |u_s| u_s \tag{5}$$

where h_W is the water depth at a cell face between the fluid and structure or the water height in the front of the structure, and u_s is the moving velocity of the structure.

[insert Figure 3.]

While the structure is treated as 3D geometry, the fluid motion is modeled as a horizontal 2D flow. Therefore, a suitable transformation technique is required to convert the 3D deformation of the structure into a 2D translation. This involves calculating the displaced water volume by the oscillating structure and then finding an equivalent distance that the structure translates in the 2D fluid simulation. The 3D structure is assumed to deform as a cantilever beam under the force applied by the actuator at a predetermined point (see Figure 4). The equivalent deformation can be derived as

$$d_{eq} = \begin{cases} \dfrac{d\,h_W^2\left(4H_M - h_W\right)}{8H_M^3} & \text{if } h_W \le H_M \\ \dfrac{d\left({H_M}^2 - 4H_M h_W + 6{h_W}^2\right)}{8H_M h_W} & \text{if } h_W > H_M \end{cases} \tag{6}$$

where d_{eq} is the equivalent deformation, and H_M is the height to the point where the deformation d is measured. Once d_{eq} is determined, the structure moving velocity u_s can be calculated by dividing the change in d_{eq} with the time interval corresponding to the deformation.

In a time step (Δt) of the flow model, the structure displacement is equal to $u_s\Delta t$, which is ensured to be smaller than the horizontal grid spacing (Δx or Δy) in the structure deformation direction. This is required by the stability of the flow model.

[insert Figure 4.]

The fluid force consists of hydrostatic and hydrodynamic components. The hydrostatic force is governed by the depth of fluid, whereas the hydrodynamic force is the result of the change in the linear momentum of fluid particles and is related to the relative velocity of the fluid and structure. Because of the non-slip condition, the fluid particles follow the structure moving and the relative velocity of fluid on the structure surface is zero. In the present 2D shallow water flow model, the hydrodynamic force on the structure surface is converted to a part of the hydrostatic force by changing the water depth in the front of the structure. For a fixed rigid structure, the hydrostatic pressure on the structure surface accounts for the stagnation pressure, which is approximately the total pressure in the approach flow. This can be explained by applying the Bernoulli equation along a streamline from the approach flow to the structure surface. Therefore, the fluid force per unit width on the structure is

$$f = \frac{1}{2}\rho g h_W^2 \tag{7}$$

where ρ is the fluid density. Integrating the fluid force over all the cells on the front surface of the structure yields the total force at each time step.

Note that the time step in the fluid model needs to satisfy the numerical stability condition and thus, may be much smaller than the sampling time step of the SFHS described in the previous section. Therefore, in a sampling step, the SW equations are solved in multiple time steps in the flow domain, and the average fluid force over these time steps is used as the input force for the structural simulation.

The used 2D shallow water flow model was tested extensively by Wu et al. (2012) using a series of experiments of dam-break flow and tsunami wave. Particularly, the model was tested using the experimental data of Synolakis (1986) on the propagation of a solitary wave over a sloping beach. Because of the HLL approximate Riemann solver used, the model can reliably simulate the wave breaking, runup and rundown on the beach. The model is further tested in the present study by comparing the calculated and measured fluid loads on a rigid block impacted by a dam-break wave. The experiment was carried out by St-Germain et al. (2012) in a flume shown in Figure 5. In the experiment, water was stored behind a gate and the gate was suddenly raised releasing the impounded water. The initial water depth behind the gate was 1.15 m, and the downstream flume bed was dry. A tall rigid block with a square cross-section (30×30 cm^2) was placed downstream of the gate. The computational domain covers the exact dimension of the flume. Uniform square cells with 5 mm grid spacing are used to discretize the flow domain, and the time step varies within the numerical stability condition (Wu et al., 2012).

Figure 6 shows the dam-break wave profiles along the centerline section of the flume in several elapsed times. The dam break wave propagates downstream with a steep front. When the wave hits the structure, the water builds up in the front of the structure. Then some water is reflected back, while some propagates around the structure. Figure 7 shows the calculated and measured fluid forces on the block. The calculated force is in good agreement with the experimental data. A sharp peak in the fluid force occurs when the wave hits the structure. Then, the fluid force reduces due to the transition from the impact load to the pseudo-hydrostatic pressure. The fluid force increases later and reaches the second peak because more water flows towards the structure. The first peak agrees with the experimental observations of Istrati (2017) and Higgins et al. (2014) when a wave initially slams a bridge structure. The present model accurately predicts the second peak, but overpredicts the first peak. This overprediction might be because the gate was lifted at a finite speed in the experiment but instantaneously in the simulation. Another reason may be that the SW equations cannot capture the complex 3D flow features in the wave front. Nevertheless, this test demonstrates that the present horizontal 2D flow model can approximately calculate the fluid force on the vertical rigid block.

[insert Figure 5.]

[insert Figure 6.]

[insert Figure 7.]

Numerical Integration Algorithm of Structure Analysis

The target responses are different in the displacement- and force-based hybrid simulations. The structure's equation of motion needs to be solved for displacement in

the displacement-based approach and for force in the force-based approach. Therefore, two different numerical integration algorithms are employed in this study.

Displacement-based approach

The α-OS method is adopted as the numerical integration algorithm to solve the structure's equation of motion for displacement (Hilber et al., 1977). The discrete form of the structure's equation of motion at time step $n+1$ is given by

$$\mathbf{M}\ddot{\mathbf{x}}_{n+1}+(1+\alpha)\mathbf{C}\dot{\mathbf{x}}_{n+1}-\alpha\mathbf{C}\dot{\mathbf{x}}_{n}+(1+\alpha)\mathbf{r}_{n+1}-\alpha\mathbf{r}_{n}=(1+\alpha)\mathbf{f}_{n+1}-\alpha\mathbf{f}_{n} \tag{8}$$

where $\mathbf{M}$ and $\mathbf{C}$ are the mass and damping matrices, respectively; $\ddot{\mathbf{x}},\dot{\mathbf{x}},\mathbf{x},\mathbf{r}$ and $\mathbf{f}$ are the acceleration, velocity, displacement, restoring force and input force vectors, respectively; α is the integration parameter; and n is the step number.

In the α-OS method, the unknown displacement vector $\mathbf{x}_{n+1}$ and velocity vector $\dot{\mathbf{x}}_{n+1}$ are obtained according to a prediction-correction procedure. In the prediction step, the following equations are used:

$$\tilde{\mathbf{x}}_{n+1}=\mathbf{x}_{n}+\Delta t\dot{\mathbf{x}}_{n}+\left(\frac{1}{2}-\beta\right)\Delta t^{2}\ddot{\mathbf{x}}_{n} \tag{9}$$

$$\tilde{\dot{\mathbf{x}}}_{n+1}=\dot{\mathbf{x}}_{n}+(1-\gamma)\Delta t\ddot{\mathbf{x}}_{n} \tag{10}$$

where $\tilde{\mathbf{x}}_{n+1}$ and $\tilde{\dot{\mathbf{x}}}_{n+1}$ are the predicted displacement and velocity vectors, respectively; β and γ are calculated based on α as $\beta=(1-\alpha)^{2}/4$ and $\gamma=(1-2\alpha)/2$; and Δt is the time step in the structure analysis, which is set as the same as the sampling time step length. The corrected displacement and velocity vectors are calculated as follows, respectively.

$$\mathbf{x}_{n+1}=\tilde{\mathbf{x}}_{n+1}+\beta\Delta t^{2}\ddot{\mathbf{x}}_{n+1} \tag{11}$$

$$\dot{\mathbf{x}}_{n+1}=\tilde{\dot{\mathbf{x}}}_{n+1}+\gamma\Delta t\ddot{\mathbf{x}}_{n+1} \tag{12}$$

The restoring force vector is approximated as

$$\mathbf{r}_{n+1}=\mathbf{K}\mathbf{x}_{n+1}+\left(\tilde{\mathbf{r}}_{n+1}-\mathbf{K}\tilde{\mathbf{x}}_{n+1}\right) \tag{13}$$

where $\mathbf{K}$ is the initial stiffness, $\tilde{\mathbf{r}}_{n+1}$ is the measured restoring force from the experiment subjected to the predicted displacement $\tilde{\mathbf{x}}_{n+1}$.

Finally, the structure's equation of motion can be formulated to obtain $\ddot{\mathbf{x}}_{n+1}$ as the solution of the following linear system:

$$\hat{\mathbf{M}}\ddot{\mathbf{x}}_{n+1} = \hat{\mathbf{f}}_{n+1} \tag{14}$$

where

$$\hat{\mathbf{M}} = \mathbf{M} + \gamma\Delta t(1+\alpha)\mathbf{C} + \beta\Delta t^2(1+\alpha)\mathbf{K} \tag{15}$$

$$\hat{\mathbf{f}}_{n+1} = (1+\alpha)\mathbf{f}_{n+1} - \alpha\mathbf{f}_n + \alpha\mathbf{r}_n - (1+\alpha)\mathbf{r}_{n+1} + \alpha\mathbf{C}\dot{\mathbf{x}}_n - (1+\alpha)\mathbf{C}\dot{\mathbf{x}}_{n+1} + \alpha(\gamma\Delta t\mathbf{C} + \beta\Delta t^2\mathbf{K})\ddot{\mathbf{x}}_n \tag{16}$$

The implementation of the above numerical algorithm is outlined in Figure 8.

[insert Figure 8.]

Force-based approach

The quadratic-alpha method developed by Forouzan (2018) is selected as the numerical integration algorithm to solve the structure's equation of motion for force. The quadratic-alpha method is a non-iterative explicit method that is specifically designed for the force-based hybrid simulation. The predicted target force is calculated based on solving the structure's equation of motion at an interpolated point as

$$\tilde{\mathbf{r}}_{n+1} = \frac{2}{\alpha(1-\alpha)}\left(\mathbf{M}\bar{\ddot{\mathbf{x}}}_n + \mathbf{C}\bar{\dot{\mathbf{x}}}_n - \tilde{\mathbf{f}}_n\right) \tag{17}$$

where

$$\tilde{\mathbf{f}}_n = \bar{\mathbf{f}}_n - \frac{1}{2}\alpha(1+\alpha)\mathbf{r}_{n-1} - (1-\alpha^2)\mathbf{r}_n \tag{18}$$

$$\bar{\mathbf{f}}_n = \frac{1}{2}\alpha(1+\alpha)\mathbf{f}_{n-1} + (1-\alpha^2)\mathbf{f}_n - \frac{1}{2}\alpha(1-\alpha)\mathbf{f}_{n+1} \tag{19}$$

$$\bar{\ddot{\mathbf{x}}}_n = \alpha\ddot{\mathbf{x}}_{n-1} + (1-\alpha)\ddot{\mathbf{x}}_n \tag{20}$$

$$\bar{\dot{\mathbf{x}}}_n = \alpha\dot{\mathbf{x}}_{n-1} + (1-\alpha)\dot{\mathbf{x}}_n \tag{21}$$

where $\tilde{\mathbf{r}}$ is the extrapolated force; and α is the interpolation parameter with the range of $0 \le \alpha \le 1$. The target restoring force $\tilde{\mathbf{r}}_{n+1}$ is used as the reference force in the force-based hybrid simulation and imposed in experimental and numerical substructures to evaluate the force-displacement relationships. The corresponding displacement $\tilde{\mathbf{x}}_{n+1}$ is then sent to the subsequent computational process to acquire the responses at step $n+1$.

The procedures in the correction step aim to exclude the unbalanced force at the end of each step. The unbalanced force in the responses at the predictor step is identified as

$$\mathbf{e}_{n+1} = -\mathbf{M}\tilde{\ddot{\mathbf{x}}}_{n+1} - \mathbf{C}\tilde{\dot{\mathbf{x}}}_{n+1} - \tilde{\mathbf{r}}_{n+1} + \mathbf{f}_{n+1} \tag{22}$$

where

$$\tilde{\ddot{\mathbf{x}}}_{n+1} = \left(1 - \frac{1}{2\beta}\right)\ddot{\mathbf{x}}_n - \frac{\dot{\mathbf{x}}_n}{\beta\Delta t} + \frac{\tilde{\mathbf{x}}_{n+1} - \mathbf{x}_n}{\beta\Delta t^2} \tag{23}$$

$$\tilde{\dot{\mathbf{x}}}_{n+1} = \dot{\mathbf{x}}_n + \left(1-\gamma\right)\Delta t\ddot{\mathbf{x}}_n + \gamma\Delta t\left\{\frac{1}{\beta\Delta t^2}\left(\tilde{\mathbf{x}}_{n+1} - \mathbf{x}_n - \Delta t\dot{\mathbf{x}}_n\right) - \left(\frac{1}{2\beta} - 1\right)\ddot{\mathbf{x}}_n\right\} \tag{24}$$

The unbalanced force formulation can be rewritten in terms of the displacement difference $\Delta\mathbf{x}_{n+1}\left(=\mathbf{x}_{n+1} - \tilde{\mathbf{x}}_{n+1}\right)$, which can be solved as

$$\Delta\mathbf{x}_{n+1} = \Phi^{-1}\mathbf{e}_{n+1} \tag{25}$$

where

$$\Phi = \frac{\mathbf{M}}{\beta\Delta t^2} + \frac{\mathbf{C}\gamma}{\beta\Delta t} + \mathbf{K} \tag{26}$$

Finally, the converged responses at step $n+1$ are updated as

$$\mathbf{x}_{n+1} = \tilde{\mathbf{x}}_{n+1} + \Delta\mathbf{x}_{n+1} \tag{27}$$

$$\dot{\mathbf{x}}_{n+1} = \tilde{\dot{\mathbf{x}}}_{n+1} + \frac{\gamma}{\beta\Delta t}\Delta\mathbf{x}_{n+1} \tag{28}$$

$$\ddot{\mathbf{x}}_{n+1} = \tilde{\ddot{\mathbf{x}}}_{n+1} + \frac{1}{\beta\Delta t^2}\Delta\mathbf{x}_{n+1} \tag{29}$$

$$\mathbf{r}_{n+1} = \tilde{\mathbf{r}}_{n+1} + \mathbf{K}\Delta\mathbf{x}_{n+1} \tag{30}$$

The responses obtained in Eqs. (27)-(30) satisfy the equilibrium conditions at step $n+1$. This entire process repeats until the end of the simulation. Figure 9 shows a flowchart of the quadratic-alpha method from an implementation viewpoint.

[insert Figure 9.]

EXPERIMENTAL SYSTEM FOR STRUCTURE-FLUID HYBRID SIMULATION

The proposed SFHS is assessed through experimental testing, which aims to investigate the functionality of the connected components (e.g., CFD, structural testing, and numerical structural model). This section presents the details of the experimental system for the SFHS, including test setup, hardware, instrumentation, and communication protocol.

Test Setup and Configuration

A schematic hardware layout for the SFHS is shown in Figure 10. The main elements include a computer running a server program with the CFD solver, a computer with LabVIEW environment as the client, data acquisition and controller, hydraulic system and test specimen. Each element is explained as follows.

[insert Figure 10.]

Server Computer: The CFD solver is written in FORTRAN and the server code is written in C++. Server and CFD exchange data using external files, which are periodically read by each program until the most recent update is found. These programs are run on a Windows-based workstation. The hybrid simulation system is run on a quasi-static manner, not real-time.

Client Computer: A hybrid simulation algorithm is implemented in the National Instruments LabVIEW on a desktop computer that serves as a client computer. The desktop computer is connected to a PXI express controller via a dedicated Ethernet cable. Communication between the desktop computer and the PXI is handled by shared variables that are built in a communication protocol in LabVIEW.

Data Acquisition and Controller: The data acquisition and control system consists of National Instruments hardware and an embedded real-time controller. The embedded controller is a 2.3 GHz high-bandwidth dual-core PXI express controller (PXIe-8130). The controller runs LabVIEW in real-time at a sampling rate of 4 kHz. For more information about hardware and software systems, refer to Nakata et al. (2014).

Hydraulic System: A fatigue-rated hydraulic actuator with a total stroke of 152 mm and a maximum dynamic loading capacity of 24.5 kN is mounted on the crossbar of the reaction frame as the loading system. The actuator is a 911D model manufactured by ShoreWestern, Inc. The actuator is equipped with a G761 series servo valve by Moog, Inc. The hydraulic power is supplied by a 114 liter-per-second Whisper Pak Model 160 from Shore Western, Inc. The hydraulic pressure is rated at 20.68 MPa (3000 psi), and a

hydraulic service manifold (HSM) with two 3.8-liter accumulators is connected to pressure and return lines.

Test specimen: The test specimen is a 1:5 scaled model of a three-story building that was damaged by the earthquake-induced tsunamis in Japan in March 2011 (Shaloudegi, 2017). The structural model has a height of 2.4 m, length of 2.0 m and width of 1.6 m as depicted in Figure 11. It has two bays along the long axis and one bay along the short axis. The frame is made of 6061-T6 aluminum I-beams that are cut to form beams and columns, which are joined together with angle bolted connections. In order to minimize any undesirable deflection of the frame, the actuator is connected to a rigid plate. Figure 12 shows a picture of the structural model.

[insert Figure 11.]

[insert Figure 12.]

Force Controller Design

To conduct the force-based hybrid simulation, a force controller is designed based on the characteristics of the experimental system using the loop shaping technique explained in detail by Nakata (2013). Figure 13 shows the frequency characteristics of the experimental system. The experimental data in Figure 13 are obtained from a system identification test conducted with band-limited white noise in a frequency range of 0-70 Hz. The analytical models are developed using the least-square curve fitting technique to capture the dynamic characteristics of the experimental data.

[insert Figure 13.]

The closed loop transfer function of the designed force controller is illustrated in Figure 14. The main concept of the controller design here is to provide control performance in a lower frequency range (from 0 to 5 Hz) and robustness in a higher frequency range, which is sufficient for the quasi-static testing.

[insert Figure 14.]

Communication Protocol between Fluid and Structure Domains

In the present study, the structural analysis is performed in a laboratory while the fluid code is executed by a computer at a different location. Therefore, the required data need to be exchanged between the two parties. The TCP/IP data communication protocol is used for sending and receiving data between two computers with a stable internet connection. The communication uses the client-server model, which is the standard method for computers to exchange information through the world wide web. After the

connection has been established between client and server, the server sends initialization data: containing simulation name, data format (decimal/binary), and other details. The client, upon receiving data, acknowledges. Thereafter the calculated force in the fluid domain is sent to the structure domain and the corresponding deformation of the structure is sent back. The data exchange continues until either party sends the termination command, or some errors are encountered in the simulation.

NUMERICAL INVESTIGATION OF THE PROPOSED STRUCTURE-FLUID HYBRID SIMULATION

Prior to the experimental demonstration, a series of numerical SFHS are performed to verify the accuracy of the connected components (e.g., CFD, and numerical structural model), as well as the functionality of the communication between the structure and fluid domains. These simulations are also essential to protect the experimental test specimen from possible unexpected damage. In these numerical hybrid simulations, the experimental substructure in the hybrid simulation is replaced with a numerical model, while the other components (such as CFD model) are unchanged. The numerical structure model uses both the displacement- and force-based approaches.

The flow simulation domain is 1,800 m long and 40 m wide, as illustrated in Figure 15. It consists of a 200 m long flat-bed deep water section, a 1,000 m long beach with a 1/20 slope, and a 600 m long dry land. The flow domain is represented with a computational mesh with a uniform cell size of 0.4 m × 0.4 m. The test structure placed on the land has a prototype dimension of 10 m in length, 8 m in width and 12 m in height. It is the prototype structure of the 1:5 scaled model specimen shown in Figure 12 used in the structural tests. Initially, the sea water level lies 1.5 m below the base of the structure. A solitary wave with an amplitude of 20 m is generated as tsunami at the seaside of the flow domain, and the outlet boundary condition is set at the land side. The Manning coefficient is given a value of 0.035 s/m$^{1/3}$.

In the numerical SFHS, the structure is modeled as a single-degree-of-freedom (SDOF) system. It is assumed to be linear. Its stiffness, natural frequency and damping ratio are 2.46×10^4 kN/m, 1.8 Hz, and 5%, respectively. The parameters in the α-OS method for the displacement-based hybrid simulation are: $\alpha = -0.3$, $\beta = 0.44$, $\gamma = 0.83$ and $\Delta t = 0.01$ s. The parameters in the quadratic-alpha method for the force-based hybrid simulation are: $\alpha = 0.5$, $\beta = 0.44$, $\gamma = 0.83$ and $\Delta t = 0.01$ s. Note that the coefficient α has different meaning and thus requires different values in the displacement- and force-based hybrid simulations, whereas the other three parameters are the same in the two simulations.

[insert Figure 15.]

The simulated wave profiles in several selected elapsed times are shown in Figure 16. The solitary wave specified at the seaside boundary transforms to an asymmetric wave as it propagates onshore. The wave front becomes steeper because the water particles at the crest have higher velocity than at the trough. The wave starts pitching and attains the onset of breaking when the wave height is about 78% of the water depth. It overturns and breaks closer to the waterline. The broken wave continues propagating over dry land like a bore, and then hits the structure. According to the model test conducted by Wu et al. (2012), the slope of the wave front is usually over-predicted because the shallow water equations cannot account for wave dispersion; however, the wave breaking and runup can be well predicted by the present model.

[insert Figure 16.]

To have a better judgment of changes in the fluid loading due to structural deformation, the fluid force on the structure is calculated in two scenarios. The first scenario assumes that the structure is rigid. The second scenario considers the flexibility of the structure and integrates the structural deformation into the fluid simulation. The fluid simulation parameters and the model structure are the same in both scenarios. Figure 17 shows the time histories of the calculated forces from the fluid simulation. Note that these results are corresponding to the full-scale structure. At the initial water impact (e.g., t<1s), the hydrodynamic force is the major contributor to the total force on the structure. As time passes, the water level in front of the structure builds up and the water velocity decreases. Consequently, the hydrodynamic force turns into pseudo-hydrostatic force. Because the velocities of the flexible structure and fluid are in the same direction in this stage, the relative water velocity and in turn the first peak in the fluid force on the flexible structure are less than those on the rigid structure (Figure 17). As time passes further, the oscillatory movement of the flexible structure alters the water height and relative velocity by pushing the water back and forth. As a result, the fluid force on the flexible structure oscillates, and the peak value is larger than that on the rigid structure. Higgins et al. (2014) and Istrati (2017) observed similar behaviors for wave forces on bridge decks. In this study, it was found that a more flexible structure induces a higher fluctuation in the fluid force, and the frequency of the force fluctuation is the same as the natural frequency of the structure.

[insert Figure 17.]

In the structure domain, the overall structural responses in the numerical SFHS are compared with a pure numerical reference. The reference is a nonlinear numerical simulation that includes an iterative process to keep the force error within tolerance. Here, the Newmark method (Newmark, 1959) is selected as the reference. For the comparison, the numerical SFHS are performed first, and then the calculated fluid force is utilized as a prescribed input force into the reference. Figure 18 (a) and (b) show the fluid force and compare the displacements calculated in the displacement-based numerical SFHS and the reference. Figure 18 (c) and (d) show the results of the force-

based numerical SFHS. The displacement time histories perfectly match between each SFHS and the reference, indicating the accuracy of the used simulation approaches in the structure domain.

[insert Figure 18.]

Figure 19 compares the calculated fluid force and displacement time histories from the displacement- and force-based numerical hybrid SFHS. In terms of fluid force, the results match each other in the entire simulation time. However, when inspected closely (Figure 19 (b)), the displacement-based numerical SFHS has slightly larger fluid force. Similar behavior is observed in the displacement time histories in Figure 19 (c). The simulation results indicate that when the structure behaves linearly, both the displacement- and force-based SFHS can capture the structure responses to the fluid loading.

[insert Figure 19.]

In addition to the above validations, a sensitivity study for the sampling time is performed to identify a good compromise between sufficient accuracy and reasonable computational effort. Three sampling times are considered: 0.005, 0.01 and 0.02 s. Figure 20 compares the fluid loads and displacements between these cases calculated from the displacement-based numerical SFHS, whereas Figure 21 shows the results from the force-based numerical SFHS. The amplitude of the fluid force with Δt=0.02 s is higher than those with Δt=0.005 and 0.01 s in both hybrid simulations. The displacements obtained with the sampling time of 0.005 and 0.01 s are very close in terms of magnitude and phase, whereas the sampling time of 0.02 s amplifies the displacement. Significant shifts in phase are observed for 0.02 s sampling time in the displacement-based numerical SFHS, but not in the corresponding force-based simulation. The force-based SFHS is less sensitive to the sampling time than the displacement-based SFHS. The simulation results illustrate the convergence of responses with the sampling time of 0.005 and 0.01 s. Therefore, the sampling time of 0.01 s is selected in the analysis, which allows the accuracy of overall results as well as the efficiency of computation time.

[insert Figure 20.]

[insert Figure 21.]

EXPERIMENTAL DEMONSTRATION OF THE PROPOSED STRUCTURE-FLUID HYBRID SIMULATION

Experimental tests are conducted on the model structure to demonstrate the feasibility of the SFHS. The flow simulation domain is the same as the previous

numerical test, shown in Figure 15. In the present experimental tests, the structure is modeled physically, and the full procedure of the SFHS is tested. In order to make the experimental condition realistic, the solitary wave height is selected such that the structure will not be overtopped in any given instance (since the shallow water model cannot accurately capture this) and the line of action of the resultant x-directional net force is always near or below the first floor where the actuator is mounted. In addition, the maximum displacement is limited within the capacity of the actuator stroke.

Figure 22 shows the time histories of fluid force and structural responses in the displacement- and force-based SFHS. The restoring force and deformation data are collected from the load cell and LVDT on the actuator that are attached to the test setup on the first floor. It is observed that the system is robust and stable in both hybrid simulations. The force-displacement relationship of the test structure is slightly nonlinear (see Figure 22 (a)). The experimental structural responses are quite different between the displacement- and force-based SFHS. The system behaves differently from the linear system numerically tested in the previous section. Therefore, the experimental results are not compared with the numerical test results.

Figure 22 (b), (c) and (d) show oscillatory behaviors in the time histories of fluid force, displacement and acceleration in both displacement- and force-based SFHS. The oscillations are weakened due to the energy dissipation of the structure. A shift lag is observed in the fluid force in the displacement-based SFHS compared with the force-based one. The displacement-based SFHS gives larger structural deformation than the force-based one does.

[insert Figure 22.]

In addition to the overall responses, the incompatible force, difference between the converged force after the correction procedure and the measured force from the experiment is investigated. A large incompatible force exists in the displacement-based SFHS, as shown in Figure 23 (a). This large incompatible force is due to the large difference between the measured and converged restoring forces shown in Figure 23 (b). The force-based approach in the hybrid simulation addresses this drawback and minimizes the force error in the experimental process by imposing a controlled force (see Figure 23 (c)). In Figure 23 (d), the measured force from the experiment is in a great agreement with the converged force, indicating the efficiency of the force-based approach in reduction of undesired incompatible force in the integration of fluid and structure simulations. The influence of the large incompatible force in the displacement-based approach propagates to the fluid simulation, while it enforces unintended nonlinearity to the system, leading to an extra deformation of the structure. This is one reason for the discrepancies in the fluid forces and structural responses between the displacement- and force-based SFHS in Figure 23.

[insert Figure 23.]

Overall, the experimental results have demonstrated the feasibility of the SFHS for structural assessment under fluid loading. Although there is no benchmark to validate the results, the physical test responses have proven that the force-based hybrid simulation provides a more accurate and realistic condition for structural assessment in the case of fluid-induced loading.

Note that since this is a pilot study, the structure is modeled as a SDOF and a fixed actuator is used. This setup cannot accommodate the changes in the location of the resultant fluid force action point due to the water level changes. Improvements can be made in the future by correcting the structure deformation considering the force acting point changes or by using multiple actuators.

CONCLUSIONS

This paper proposed a structure-fluid hybrid simulation for structural assessment under hydrodynamic loading. The fluid loading at each sampling time step is calculated by solving the 2D shallow water equations. Then, the calculated fluid loading is sent to the structure domain as the input force, and the structure responses are obtained through a hybrid simulation procedure. The structure deformation is used as the boundary condition to calculate the fluid loading in the next sampling step. In this way, the interaction of fluid and structure is incorporated into the simulation and the fluid loading and structural deformation are coupled.

While hybrid simulation is a powerful technique for seismic assessment, it has some limitations for tsunami loading. One of the limitations is due to the unavoidable error between the measured and converged restoring forces caused by high noise in the force-feedback control, designated as incompatible force, in the conventional displacement-based hybrid simulation. To address this limitation, a force-based hybrid simulation is adopted in this study for structural simulation. To investigate the influence of the incompatible force on the accuracy of overall responses, the structure-fluid hybrid simulation is performed with both displacement- and force-based approaches.

Numerical investigations are performed to test the accuracy of the connected components (e.g., CFD, and numerical structural model) as well as the functionality of the communication between the structure and fluid domains. Subsequently, the entire proposed SFHS is physically tested using a 1:5 scaled model structure while the tsunami wave loading is calculated with a CFD model. The tests demonstrated the feasibility of running both displacement- and force-based SFHS with the fluid simulation. However, the level of incompatible force in the displacement-based approach is high and affects the fidelity of the simulation results. The force-based approach is capable of reducing the incompatible force, allowing for more realistic and reliable structural assessment under tsunami loading.

ACKNOWLEDGEMENT

This research is supported by the U.S. National Science Foundation under grant number CMMI-1463024 (Advanced Hybrid Simulation for Storm Surge Loads).

REFERENCES

Dermitzakis SN and Mahin SA (1985) Development of Substructuring Techniques for On-line Computer Controlled Seismic Performance Testing. *Earthquake Engineering Research Center*, College of Engineering, University of California, USA.

Forouzan B (2018) Force-Based Hybrid Simulation for Structural Assessment to Coastal Hazards. *PhD Thesis*, Clarkson University, USA.

Hakuno M, Shidawara M, and Hara T (1969) Dynamic Destructive Test of a Cantilever Beam, Controlled by an Analog-Computer. *Proceedings of the Japan Society of Civil Engineers* 1969(171): 1–9.

Harten A, Lax PD, and Van Leer B (1983) On Upstream Differencing and Godunov-Type Schemes for Hyperbolic Conservation Laws. *SIAM Review* 25(1): 35–61.

Higgins C, Lehrman J, Bradner C, Schumacher T and Cox D (2014) Hybrid Testing of a Prestressed Girder Bridge to Resist Wave Forces. *29th US-Japan Bridge Engineering Workshop*, Tsukuba, Japan.

Hilber HM, Hughes TJR, and Taylor RL (1977) Improved Numerical Dissipation For Time Integration Algorithms in Structural Dynamics. *Earthquake Engineering and Structural Dynamic* 5(3): 283–292.

Istrati D (2017) Large-Scale Experiments of Tsunami Inundation of Bridges Including Fluid-Structure-Interaction," *PhD Thesis*, University of Nevada, Reno.

Kareem A (1990) Measurements of Pressure and Force Fields on Building Models in Simulated Atmospheric Flows. *Journal of Wind Engineering and Industrial Aerodynamic* 36(1) 589–599.

Kareem A (2008) Numerical Simulation of Wind Effects: A Probabilistic Perspective. *Journal of Wind Engineering and Industrial Aerodynamic* 96(10): 1472–1497.

Kato Y and Kanda M (2014) Development of A Modified Hybrid Aerodynamic Vibration Technique for Simulating Aerodynamic Vibration of Structures in A Wind Tunnel. *Journal of Wind Engineering and Industrial Aerodynamic* 135: 10–21.

Nakata N (2013) Effective Force Testing Using A Robust Loop Shaping Controller. *Earthquake Engineering and Structural Dynamic* 42(2): 261–275.

Nakata N, Krug E, and King A (2014) Experimental Implementation And Verification of Multi-Degrees-of-Freedom Effective Force Testing. *Earthquake Engineering and Structural Dynamic* 43(3): 413–428.

Newmark NM (1959) A Method of Computation for Structural Dynamics. *Journal of Engineering Mechanics Division* 85(3): 67–94.

Nistor I, Palermo D, Cornett A and Al-Faestly T (2011) Experimental And Numerical Modeling Of Tsunami Loading On Structures. *Coastal Engineering Proceedings* 1(32).

Shaloudegi K (2017) Design of a 1/5th-Scale Frame Structure and Experimental Demonstration of Hybrid Simulation," *Master Thesis*, Clarkson University, USA.

Shing PB and Mahin SA (1990) Experimental Error Effects In Pseudodynamic Testing. *Journal of Engineering Mechanics* 116(4):805-821.

St-Germain P, Nistor I, and Townsend R (2012) Numerical Modeling of the Impact with Structures of Tsunami Bores Propagating on Dry and Wet Beds Using the SPH Method. *International Journal of Protective Structures* 3(2): 221–255.

Synolakis CE (1986) The Run up of Long Waves. *PhD Thesis*, California Institute of Technology, USA.

Takanashi K and Nakashima M (1987) Japanese Activities on On-Line Testing. *Journal of Engineering Mechanics* 113(7): 1014-1032.

Tamura Y, Suganuma S, Kikuchi H and Hibi K(1999) Proper Orthogonal Decomposition of Random Wind Pressure Field. *Journal of Fluids and Structure* 13(7): 1069–1095.

Thewalt CR and Mahin SA (1987) Hybrid Solution Techniques for Generalized Pseudodynamic Testing. *Earthquake Engineering Research Center*, College of Engineering, University of California, USA.

Titov V and Synolakis CE (1995) Modeling of Breaking and Nonbreaking Long-Wave Evolution and Runup Using VTCS-2. *Journal of Waterway, Port, Coastal and Ocean Engineering* 121(6): 308–317.

Titov V and Synolakis CE (1998) Numerical Modeling of Tidal Wave Runup. *Journal of Waterway, Port, Coastal and Ocean Engineering* 124(4): 157–171.

Wei Z, Dalrymple RA, Hérault A, Bilotta G, Rustico E and Yeh H (2015) SPH Modeling of Dynamic Impact of Tsunami Bore on Bridge Piers. *Coastal Engineering* 104: 26–42.

Winter AO, Motley MR and Eberhard MO (2018) Tsunami-Like Wave Loading Of Individual Bridge Components. *Journal of Bridge Engineering* 23(2) 04017137.

Wu W, Marsooli R, and He Z (2012) Depth-Averaged Two-Dimensional Model of Unsteady Flow and Sediment Transport due to Noncohesive Embankment Break/Breaching. *Journal of Hydraulic Engineering* 138(6): 503–516.

Yang G, Causon DM, Ingram DM, Saunders R and Battent P (1997) A Cartesian Cut Cell Method for Compressible Flows Part A: Static Body Problems. *Aeronautical Journal* 101(1002): 47–56.

Yang G, Causon DM, and Ingram DM (2000) Calculation of Compressible Flows About Complex Moving Geometries Using a Three-dimensional Cartesian Cut Cell Method. *International Journal of Numerical Methods in Fluids* 33(8): 1121–1151.

Yeh H (1994) Propagation and Amplification of Tsunamis at Coastal Boundaries. *Nature* 372(6504): 353.